Available online at www.sciencedirect.com
SCIENCE DIRECT®
International Journal of Multiphase Flow 30 (2004) 649–673
International Journal of Multiphase Flow
www.elsevier.com/locate/ijmulflow

Simulation of particles released near the wall in a turbulent boundary layer

A.J. Dorgan, E. Loth *

Department of Aeronautical and Astronautical Engineering, University of Illinois at Urbana-Champaign, 306 Talbot Laboratory, 104 South Wright Street, Urbana, IL 61801-2935, USA

Received 15 July 2003; received in revised form 9 May 2004

Abstract

A direct numerical simulation was used along with a Lagrangian particle tracking technique to study particle motion in a horizontal, spatially developing turbulent boundary layer along an upper-wall (with terminal velocity directed away from the wall). The objective of the research was to study particle diffusion, dispersion, reflection, and mean velocity in the context of two parametric studies: one investigated the effect of the drift parameter (the ratio of particle terminal velocity to fluid friction velocity) for a fixed and finite particle inertia, and the second varied the drift parameter and particle inertia by the same amount (i.e. for a constant Froude number). A range of drift parameters from 10^{-4} to 10^{0} were considered for both cases. The particles were injected into the simulation at a height of four wall units for several evenly distributed points across the span and a perfectly elastic wall collision was specified at one wall unit.

Statistics collected along the particle trajectories demonstrated a transition in particle movement from one that is dominated by diffusion to one that is dominated by gravity. For small and intermediate sized particles (i.e. ones with outer Stokes numbers and drift parameters much less than unity) transverse diffusion away from the wall dominated particle motion. However, preferential concentration is seen near the wall for intermediate-sized particles due to inhomogeneous turbulence effects (turbophoresis), consistent with previous channel flow studies. Particle–wall collision statistics indicated that impact velocities tended to increase with increasing terminal velocity for small and moderate inertias, after which initial conditions become important. Finally, high relative velocity fluctuations (compared to terminal velocity) were found as particle inertia increased, and were well described with a quasi-one-dimensional fluctuation model.

* Corresponding author. Tel.: +1-217-244-5581.
E-mail address: e-loth@uiuc.edu (E. Loth).

0301-9322/$ - see front matter © 2004 Published by Elsevier Ltd.
doi:10.1016/j.ijmultiphaseflow.2004.05.006

1. Introduction

Particle motion in a horizontal turbulent boundary layer with a gravitationally-induced terminal velocity away from the wall is important to several external flows, e.g. particles ablating or released just below an aerodynamic surface. Some of the primary parameters that control particle diffusion in a turbulent boundary layer include the drift parameter, the Stokes number (based on either outer scales or wall scales), the Froude number, and the Reynolds number. Herein, the drift parameter, γ, is defined as the ratio of particle terminal velocity (V_{term}) to the wall friction velocity of the fluid (u_τ), the outer Stokes number (St_δ) is the ratio of particle response time (τ_p) to a large eddy time scale ($\tau_\delta = \delta/u_\tau$), the wall Stokes number (St^+) is the ratio of τ_p to a wall time-scale ($\tau_f^+ = \nu_f/u_\tau^2$), Fr_δ is an outer Froude number relating convection to gravitation and is based on the boundary layer thickness, Re_δ is the Reynolds number of the continuous phase based on the boundary layer thickness, Re_p is the particle Reynolds number based on the relative velocity, and $Re_{p,\text{term}}$ is the particle Reynolds number based on the particle's terminal velocity:

$$\gamma = \frac{V_{\text{term}}}{u_\tau}, \quad St_\delta = \frac{\tau_p}{\tau_\delta} = \frac{\tau_p}{(\delta/u_\tau)}, \quad St^+ = \frac{\tau_p}{\tau_f^+} = \frac{\tau_p}{\left(\nu_f/u_\tau^2\right)}, \quad Fr_\delta = \frac{u_\tau^2}{g\delta}$$
$$Re_\delta = \frac{U_\infty \delta}{\nu_f}, \quad Re_p = \frac{|V_{\text{rel}}| d_p}{\nu_f}, \quad Re_{p,\text{term}} = \frac{V_{\text{term}} d_p}{\nu_f} \tag{1}$$

where ν_f is the fluid kinematic viscosity, U_∞ is the free-stream velocity, δ is the reference boundary layer thickness, g is the acceleration of gravity, and $\mathbf{V}_{\text{rel}}$ is $\mathbf{V}_p - \mathbf{V}_f$ (whose magnitude is equal to V_{term}, in quiescent conditions). Assuming a linear drag-law (i.e. small particle Reynolds numbers) and negligible added mass (i.e. the particle density is much greater than the fluid density), the particle response time is given as $\tau_p = V_{\text{term}}/g$. In this case, a linear relationship exists between the Stokes number, Froude number, and the drift parameter, i.e. $St_\delta = \gamma Fr_\delta$.

The fluid's integral time scale (τ_Λ) is based on the streamwise fluid velocity decorrelation integral (to be defined in Section 2.3) and tends to be bounded by τ_δ and τ_f^+. For long-time ($t \gg \tau_p$ and $t \gg \tau_\Lambda$) particle diffusion in homogeneous isotropic turbulence, previous experimental and numerical studies have shown that γ (via the crossing trajectory effect) is the main controlling parameter (Stock, 1996; Loth, 2000). In particular, the long-time diffusion rate for $\gamma \ll 1$ is locally similar to that of a tracer particle, while the diffusion rate reduces as approximately γ^{-1} for large drift parameters.

While the influence of the Stokes number is weak for long-time diffusion, it can significantly reduce the rate of diffusion for short-times ($t \ll \tau_\Lambda$) when large Stokes numbers are considered. This is grounded in the physical nature of large inertia particles as the dispersion is not strongly affected by individual turbulent structure events, e.g. an eddy or a boundary layer ejection. (Herein, "diffusion" refers to mean-spread of the particle cloud, and "dispersion" refers to particle motion associated with an individual spatial/temporal turbulent structure.)

Particle diffusion and dispersion in inhomogeneous turbulent flows introduces additional complexity (as compared to that in homogeneous turbulence). Kaftori et al. (1995) experimentally studied the motion of nearly neutrally buoyant particles near the wall of a spatially-evolving boundary layer for a range of St^+ from 0.2 to 18, in which the particles do not deposit on the wall but rather rebound as they make contact. The study found that particles concentrated in regions of slow-moving fluid near the wall, i.e. exhibited "wall-peaking". Young and Leeming (1997)

noted that this phenomenon of wall-peaking is due to "turbophoresis" (a convective drift of particles down gradients of mean-square fluctuating velocity) and could be approximately modeled as a function of the Stokes number.

As discussed by Dorgan (2003) and overviewed below, direct numerical simulation (DNS) has allowed researchers more insight into the particle dynamics and deposition for pipe and channel flows, where inhomogeneous effects can be strong close to the wall. Brooke et al. (1992) considered a DNS test matrix consisting of St^+ values ranging from 3 to 10 for a channel flow. Their study noticed that particles tend to concentrate in the viscous sublayer where they are trapped in coherent streamwise structures (horseshoe vortices) which push the particles toward the wall. Similarly, Pedinotti et al. (1992) observed preferential concentration in the low-speed streaks near a DNS channel wall where the effect was most noticeable for the intermediate inertia values (i.e. St^+ on the order of 3) but lessened when gravity was absent. Marchioli and Soldati (2002) observed particle simulations for a DNS vertical channel in an attempt to understand the mechanisms responsible for increasing the particle concentration in the near-wall region. The study suggested that the Stokes number may be the more important parameter for the near near-wall dynamics (consistent with the model of Young and Leeming, 1997).

There are several differences between the above DNS studies and the present study. Firstly, of the DNS studies discussed above, none is for a canonical, spatially growing boundary layer (as in the present case) and none consider as large an Re_τ value (270 in the present study). Secondly, none of the studies consider such a large range of γ for both a fixed Froude number (consistent with changing particle size in a fixed continuous flow) and a fixed Stokes number (to separate the inertia and drift parameter effects). The latter study is not easily replicated experimentally—though Wells and Stock (1983) used an electromagnetic field to achieve some aspects of this condition. Thirdly, the present research considers the injection of particles near the wall (at $y^+ = 4$), whereas most previous studies start with particles initially distributed uniformly throughout the computational domain, injected at random points in the domain, or injected at the centerline. Fourthly, the streamwise recycling of particle injections often used in channel flows is not used herein since the flow, and thus particle concentration, is *spatially developing*. Finally, most of the studies focused on deposition, whereas an elastic reflection condition is considered herein.

For these unique flow and particle conditions, we examine particle diffusion, dispersion, reflection, and velocity statistics. It should be noted that detailed turbulence and flowfield Eulerian statistics of the turbulent boundary layer are available (Dorgan, 2003). As such, RANS-based numerical particle diffusion techniques (e.g. Lagrangian random walk models and Eulerian diffusion transport models) can be validated with the present data for a well-characterized inhomogeneous, anisotropic flow (not subject to experimental uncertainties or RANS empiricism).

2. Methodology

2.1. Turbulent boundary layer

The continuous-phase solution for the turbulent boundary layer was obtained from a DNS of the incompressible Navier–Stokes equations. The continuous-phase solution is independent of the

particle trajectories as the particle concentration is assumed to be dilute and does not affect the carrier phase (i.e. the flow only allows one-way coupling of the fluid on the particle motion). The DNS code was developed by Spalart and Watmuff (1993) to simulate a three-dimensional, spatially developing boundary layer with zero streamwise pressure gradient. The method is spectrally-accurate in the three spatial directions and second-order accurate in time. The solution domain is semi-infinite over a flat, smooth surface with $0 \leqslant x \leqslant \Lambda_x$, $0 \leqslant z \leqslant \Lambda_z$, and $0 \leqslant y \leqslant \infty$ where x, z, and y represent the streamwise, spanwise, and transverse directions and where Λ_x is the streamwise domain length and Λ_z is the length of one period of the periodic spanwise domain. The domain is discretized by 256 nodes in the stream direction, 96 in the span direction, and 55 in the transverse direction for a total of 1,351,680 nodes in the three-dimensional mesh. Spatial evolution aspects and time integration details are given by Dorgan and Loth (2003).

Eulerian statistics of the fluid properties are shown in Fig. 1 for transverse profiles of the mean velocity, turbulent kinetic energy, and transverse velocity fluctuations at $x = \Lambda_x/3$ (additional data is given by Dorgan, 2003). The Eulerian-averaged properties in this figure are denoted by $[\ldots]$ and represent averaging over a period of the spanwise domain and time of about 10 τ_δ for each transverse nodal location at this streamwise position. In Fig. 1a, the mean velocity profile is normalized by u_τ and there is evidence of the viscous sublayer below $y^+ \sim 20$ and a transition to a logarithmic curve by $y^+ \sim 50$. The boundary layer edge is located at roughly $y^+ = 270$ (i.e. $Re_\tau = 270$) and comparison with the common "law of the wall" expressions for high Reynolds number boundary layers show similar behavior. Fig. 1b shows the turbulent kinetic energy (k) profile normalized by u_τ^2. Below $y^+ = 1$, the energy is nearly zero and approaches a maximum of

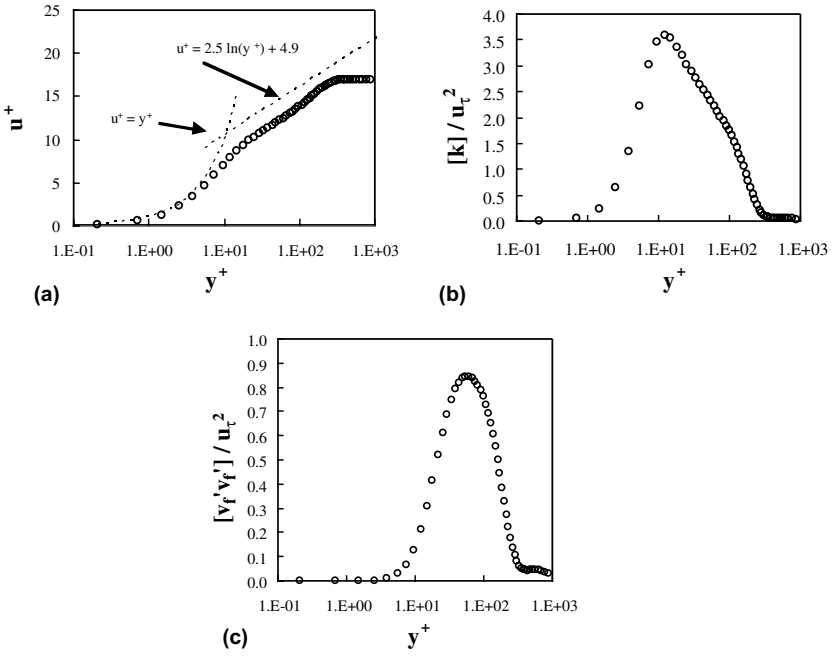

Fig. 1. DNS statistics at $\Lambda_x/3$ for (a) the mean velocity profile, (b) the turbulent kinetic energy profile and (c) the transverse velocity fluctuation autocorrelation.

about 3.6 at around y^+ of 15, then approaches zero toward the boundary layer edge. This is qualitatively consistent with the experiments of Klebanov at $Re_\tau = 2800$ as reported by Hinze (1959) with a peak of $6u_\tau$ at a y^+ of about 22. The transverse velocity fluctuations represent the smallest component of k such that $[v'_f v'_f]$ peaks at a magnitude of only $0.9u_\tau$ at y^+ of about 70. In comparison, the Klebanov data indicated a peak $[v'_f v'_f]$ of $0.92u_\tau$, a magnitude also consistent with experimental pipe flow and DNS data reported by Young and Leeming (1997). The location for the peak transverse velocity fluctuation is about 60 for the present results but varies substantially in the literature, e.g. about 280 for the data cited by Hinze but about 50 for the data cited by Young and Leeming (1997).

2.2. Particle equation of motion

The Lagrangian equation of motion for a heavy, rigid particle used herein is given by

$$\rho_p \frac{d\mathbf{V}_p}{dt} = -18\rho_f \nu_f \frac{\mathbf{V}_{rel}}{d_p^2} + \rho_p \mathbf{g} \tag{2}$$

where d_p is the particle diameter, and ρ_p and ρ_f are particle and fluid densities, respectively. In this expression, ρ_p was assumed to be much greater than ρ_f such that other forces, such as the lift force (which acts perpendicular to both the drag force and the vorticity of the fluid), the stress gradient force (which accounts for gradients in the pressure and shear stress in the fluid surrounding the particle), and the Basset history force (which is associated with the temporal delay in the boundary layer development on the particle) may be assumed negligible. The first term on the RHS represents the Stokesian drag force and the second term is due to the buoyancy force with $\mathbf{g}$ representing the gravity vector. A linear drag law has been employed as it avoids the non-linearities and empiricism associated with high Reynolds number expressions. In addition, the particles are treated as point-volumes and rotation and shear effects are neglected. These assumptions were employed to focus the study on drag, inertia, and gravitational effects.

The particle trajectories are computed by numerically integrating the particle equation of motion. The integration is performed using a modified version of the exponential-Lagrangian method as described by Barton (1996) and discussed by Dorgan (2003). The exponential-Lagrangian scheme is given by

$$\mathbf{V}_p(t+\Delta t) = \mathbf{V}_p(t)\exp\left(-\Delta t/\tau_p\right) + \left[1-\exp\left(-\Delta t/\tau_p\right)\right]\tau_p \ * \left(\frac{1}{\tau_p}\mathbf{V}_f + \mathbf{g}\right) \tag{3}$$

The exponential-Lagrangian schemed was implemented in an Adams–Bashforth, predictor–corrector fashion for second-order accuracy in time. To find the average fluid velocity along the trajectory, an eight-node isoparametric hexahedron was utilized with tri-linear interpolation.

2.3. Test conditions

The baseline test condition for the particle/turbulent boundary layer interaction was chosen as $St_\delta = 10^{-2}$ and $\gamma = 10^{-2}$ (and thus a Froude number of unity). This is consistent with a 24 μm diameter solid sphere with a density of 1000 kg/m^3 in a flow of air with $\delta = 22$ cm and $u_\tau = 1.47$ m/s (Re_τ of approximately 22,000). In this case, the particle radius is equal to one wall unit, and

elastic reflection with the wall occurs when the transverse location of the particle centroid (y_p^+) equals one.

The test conditions for the constant inertia study are centered on the baseline condition and used a range of five drift parameters varying from 10^{-4} to 10^0, all for the baseline St_δ of 10^{-2} ($St^+ = 2.7$). This St_δ value (10^{-2}) ensures that inertial effects are small (i.e. the particle is able to effectively respond to the *majority* of the fluid structures in the boundary layer but does not simply behave as a passive scalar in the near-wall region). Since Stokes number is held constant, the exclusive effect of varying the drift parameter can be isolated. The test conditions for the constant Fr_δ study include seven different cases all with $Fr_\delta = 1$, where $St_\delta = \gamma$ through a range of γ from 10^{-4} to 10^0. In both studies, the baseline test condition described above represents the center of the γ range as viewed on a logarithmic scale (Table 1a) where the wall Stokes number, St^+, is seen to be much larger than the outer Stokes number, St_δ.

In order to assess a local Stokes number, the transverse distribution of the fluid integral time-scale was first obtained. The streamwise integral Lagrangian time-scale of the fluid ($\tau_{\Lambda,u}$) is defined with the decorrelation of the streamwise velocity fluctuations (u'_f)

$$\tau_{\Lambda,u}(y) = \int_0^\infty \langle u'_f(t)u'_f(t+\tau)\rangle \, d\tau / \langle u'_f(t)^2\rangle \tag{4}$$

where

$$u'_f(x,y,z,t) = u_f(x,y,z,t) - [u_f(x,y)] \tag{5}$$

Several DNS runs were conducted to find the above Lagrangian decorrelation for a fluid tracer ($u_p = u_f$) injected at various transverse locations. Similarly, $\tau_{\Lambda,v}$ and $\tau_{\Lambda,w}$ were obtained and the three time-scales averaged together to give τ_Λ as a function of y^+ (Bocksell, 2003). The local Stokes number, $\langle St_\Lambda \rangle$, can then be calculated based on the particle-observed fluid integral time

Table 1
Particle conditions for (a) constant Stokes number study and (b) constant Froude number study

γ	St_δ	$\langle St_\Lambda \rangle$	St^+	τ_{dom}/τ_Λ	τ_{dom}/τ_p
(a)					
1×10^{-4}	1×10^{-2}	9.74E−02	2.7E+00	21.0	216
1×10^{-3}	1×10^{-2}	9.46E−02	2.7E+00	19.7	208
1×10^{-2}	1×10^{-2}	8.33E−02	2.7E+00	14.6	176
1×10^{-1}	1×10^{-2}	6.66E−02	2.7E+00	9.2	138
1×10^{0}	1×10^{-2}	4.74E−02	2.7E+00	4.9	103
(b)					
1×10^{-4}	1×10^{-4}	8.3E−04	2.7E−02	14.8	17695
1×10^{-3}	1×10^{-3}	8.3E−03	2.7E−01	14.6	1757
1×10^{-2}	1×10^{-2}	8.3E−02	2.7E+00	14.6	176
3.16×10^{-2}	3.16×10^{-2}	2.6E−01	8.4E+00	14.4	55
1×10^{-1}	1×10^{-1}	7.9E−01	2.7E+01	12.6	16
3.16×10^{-1}	3.16×10^{-1}	2.0E+00	8.4E+01	9.3	5
1×10^{0}	1×10^{0}	4.5E+00	2.7E+02	7.4	2

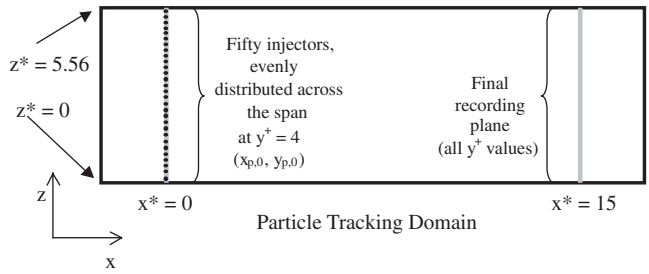

Fig. 2. Illustration of the particle injection location as well as the particle tracking domain. Note that the injection locations correspond to x_{p0}, y_{p0}, z_{p0}.

scale, $\tau_\Lambda(y^+)$, i.e. sampled along the particle path. Table 1 shows that $\langle St_\Lambda \rangle$ is bounded by St_δ and St^+.

The particles were injected with the sum of the mean fluid velocity and the terminal velocity, i.e. with $u_p = [u_f]$ (approximately $4u_\tau$), $v_p = [v_f] + V_{term}$, and $w_p = [w_f] = 0$ (where u, v, and w represent the streamwise, vertical, and spanwise velocity components, respectively and where $(\ldots)_p$ and $(\ldots)_f$ distinguish particle velocities from fluid velocities). This choice of injection (as opposed to injecting at the *instantaneous* fluid velocity plus the terminal velocity) ensured that the particles with the largest Stokes numbers would not possess unrealistically large initial velocity variations that are generally inconsistent with their long response times. In order to prevent wall collisions from acting as the dominant diffusion phenomena for the larger particles, the particle's terminal velocity is directed away from the wall. A perfectly elastic wall collision at y^+ of 1 was imposed as a reflection condition (consistent with the baseline physical particle dimensions) so that the particles would move downstream in a reasonable time period regardless of the Stokes number.

The particles were injected at uniform spanwise locations at $y^+ = 4$ and $x = \Lambda_x/3$ and tracked through a distance of 15 boundary layer thicknesses downstream (Fig. 2). Fifty particles were injected every other time-step (i.e. at every $0.57\tau_f^+$) for a period of 4000 time steps ($4.38\tau_\delta$) such that a total of 100,000 particles were injected (large enough for converged statistical results). The streamwise injection location corresponds to $Re_\delta = 4500$ and $Re_\tau \approx 270$. The streamwise portion of this particle tracking region was non-dimensionalized with respect to the reference boundary layer thickness as $0 \leqslant x^* \leqslant 15$, where $x^* = (x - \Lambda_x/3)/\delta$ and the reference boundary layer thickness, δ, is the thickness at $\Lambda_x/3$. Similarly, the spanwise domain was non-dimensionalized by δ to obtain $0 \leqslant z^* \leqslant 5.56$, where $z^* = \Lambda_z/\delta$.

3. Results

3.1. Flow-visualization

In order to identify how the particles interact with the carrier phase, several instantaneous snapshots of the simulation were obtained for the various conditions considered. In the following figures, the particle positions are mapped onto the streamwise velocity field for a given spanwise location. The fluid solution corresponds to $z^* = 2.78$ (the center of the span) and the particles

(shown as black dots) are located in a range surrounding the fluid plane from $2.60 \leqslant z^* \leqslant 2.95$. This limited spanwise range for particle positions was chosen to be large enough to include a significant number of particles for the visualization, but at the same time remain sufficiently small to insure that the selected fluid plane is a good representation of the fluid solution in the neighborhood of the actual particle location. Fig. 3 gives visualizations of the constant Stokes number simulation for the particle conditions $\gamma = 10^{-4}$, 10^{-1}, and 10^{0} with $St_\delta = 10^{-2}$. Fig. 4

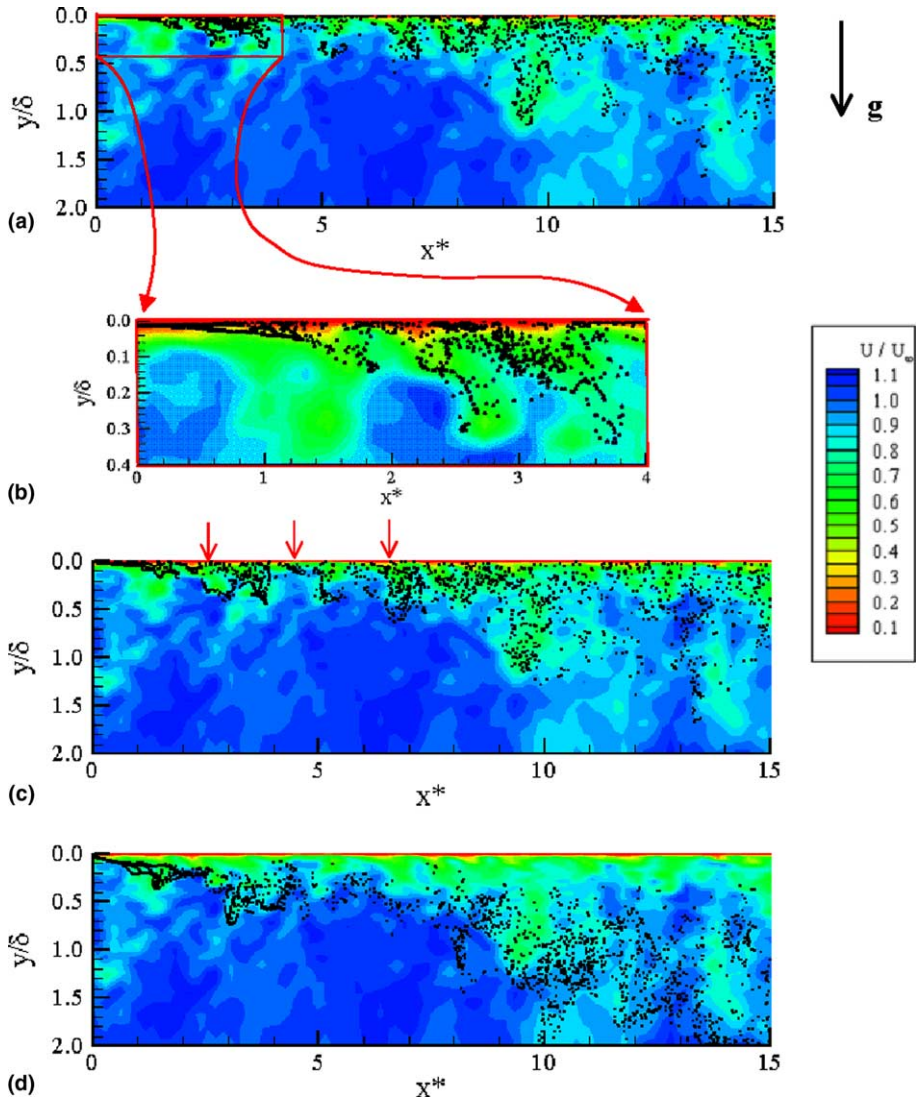

Fig. 3. Instantaneous streamwise distribution (color range) with particle locations (shown as black dots) with constant $St_\delta = 10^{-2}$ for (a) $\gamma = 10^{-4}$, (b) $\gamma = 10^{-4}$ but with a magnified view of the red box seen in (a), (c) $\gamma = 10^{-1}$ (red arrows indicate wall sweeps), and (d) $\gamma = 10^{0}$. (For interpretation of the references in colour in this figure legend, the reader is referred to the web version of this article.)

shows the visualizations of the constant Froude number study for the $\gamma = 10^{-4}$, 10^{-1}, 0.316, and 10^{0} cases with $Fr_{\delta} = 1$. Note comparisons between the two studies for the same γ (e.g. 10^{-4}, 10^{-1}, 10^{0}) would indicate differences due to the Stokes number.

First, the constant Stokes number study shown in Fig. 3 will be discussed. In looking at the close-up picture for the $\gamma = 10^{-4}$ case (Fig. 3b), it is noted that the particle ejections tend to correspond to boundary layer ejections from the near-wall region, i.e. low-speed fluid thrusting into the outer region of the boundary layer. This preferential concentration is expected as boundary layer ejections should be the primary mechanism for moving particles rapidly away from the wall. As the particles move farther downstream (and away from the wall) the correlation

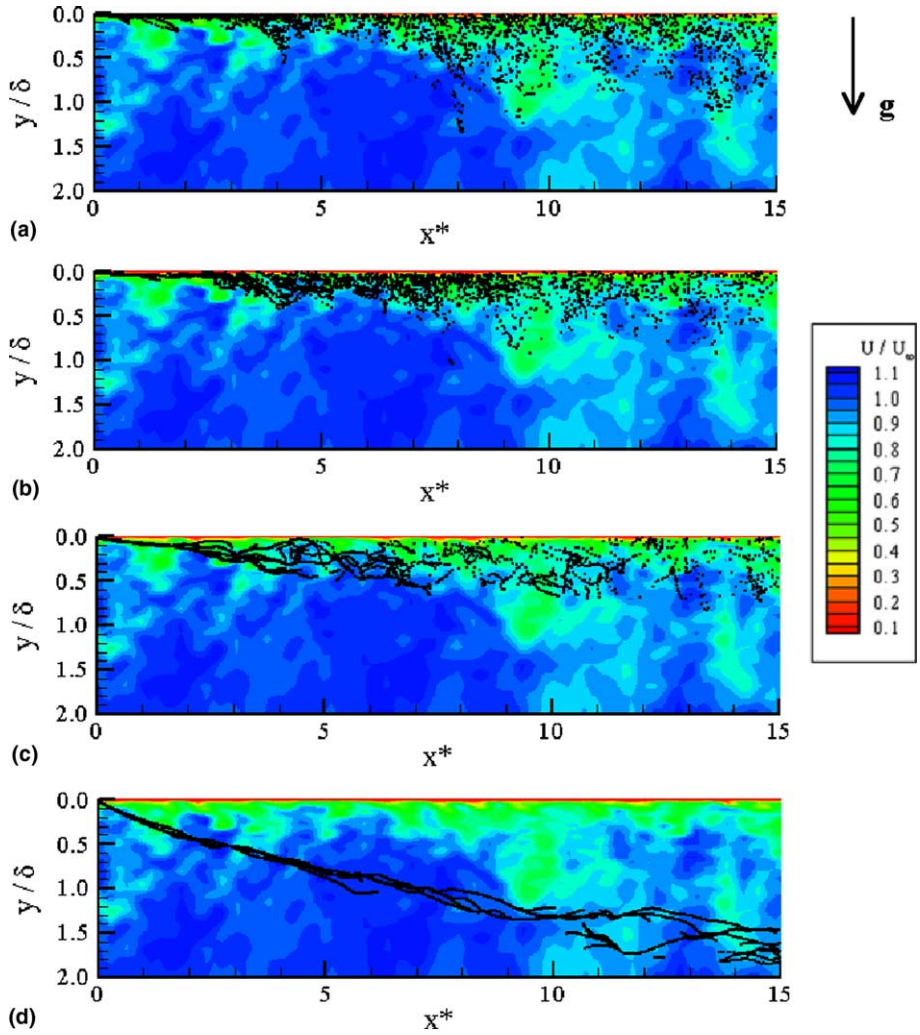

Fig. 4. Instantaneous streamwise distribution (color range) with particle locations (shown as black dots) with constant $Fr_{\delta} = 1$ for (a) $\gamma = 10^{-4}$, (b) $\gamma = 10^{-1}$, (c) $\gamma = 3.16 \times 10^{-1}$, and (d) $\gamma = 10^{0}$. (For interpretation of the references in colour in this figure legend, the reader is referred to the web version of this article.)

between the fluid structures and the particle location tends to be reduced but is still significant (Fig. 3a). In addition to this mechanism for particle movement, sustained near-wall concentration is also evident in the low-speed regions close to the wall. This particle condition has sufficient inertia ($St^+ = 2.7$) to experience preferential concentration in the near-wall region through the process of turbophoresis. As noted by Marchioli and Soldati (2002), the mechanism responsible for high near-wall concentrations of inertial particles is the superior effectiveness of wall-sweep structures moving particles to the wall as opposed to boundary layer ejections removing particles from the near-wall region.

The $\gamma = 10^{-1}$ (Fig. 3c) case shows effects of the increased terminal velocity. The level of near-wall concentration is reduced as the particles are more effectively pulled from the near-wall structures (i.e. the terminal velocity is strong enough to overcome the effects of turbophoresis). Far downstream ($x^* > 10$) the particles tend to be in the outer-region of the boundary layer and show less correlation with low-speed fluid pockets ejected from the wall than noted for the $\gamma = 10^{-4}$ case. This is attributed to the increased crossing-trajectory effect whereby particles cut through eddies instead of remaining trapped inside them. An interesting phenomenon shown in Fig. 3c are tongues of high speed fluid (wall sweep structures) forcing particles back to the wall at x^* locations of approximately 2.5, 4.5, and 6.5 (see red arrows). Fig. 3d gives the snapshot of the $\gamma = 10^0$ simulation. The particles are seen to immediately leave the transverse injection location and enter the outer regions of the boundary layer due to the particle's higher terminal velocity. However, the cloud disperses as much as is seen in the lower drift parameter case due to the constant Stokes number condition.

As mentioned above, the constant Froude number results are shown in Fig. 4 for four selected test conditions. Fig. 4a shows a visualization taken from the $St_\delta = \gamma = 10^{-4}$ case ($St^+ = 0.027$)—the nearly tracer particle case. After the particles move from the injection location where the concentration is necessarily compact, it is noted that the particles are more uniformly distributed across a portion of the boundary layer than in Fig. 3b (i.e. less correlation is noticed between particle location and fluid structure than in the case shown in Fig. 3a where $St^+ = 2.7$). This is attributed to their tendency to exhibit fluid tracer diffusion characteristics since turbophoresis and preferential concentration effects are negligible due to a lack of particle inertia (Wang and Maxey, 1993, Young and Leeming, 1997).

In Fig. 4b ($\gamma = 10^{-1}$ and $St_\delta = 10^{-1}$) the particles maintain a stronger near-wall concentration despite their increase in terminal velocity. As the particles in this test case have a St^+ of 27 they are difficult to remove from the near-wall structures (i.e. γ is not sufficiently large to pull the particles from the near-wall structures). This is consistent with the fact that the large particle ejections (e.g. $x^* = 3.5$) correspond to previous large fluid ejections from the boundary layer. In comparing the $\gamma = 10^{-1}$ cases of Figs. 3c and 4b, it is obvious that the higher Stokes number in the latter case yields much less diffusion, which is attributed to the increased inertia.

Fig. 4c and d show the $St_\delta = \gamma = 0.316$ and $St_\delta = \gamma = 1.0$ cases, respectively, where the increased particle inertia and crossing trajectory effect are quite evident in that the correlation with flow structures is reduced. For each case, all the particles tend to leave the injection location on a similar trajectory (especially for $\gamma = St_\delta = 1$) for a significant distance. After some downstream location, several different trajectories can be identified but the particles fail to become strongly diffused. In the $\gamma = 1$ case, it can be seen that the particles do not initiate significant diffusion until near the mean boundary layer edge. In comparing Figs. 3d and 4d, it is seen that both cases yield

the same net transverse rise velocity for the particle cloud, but the condition in Fig. 4d shows much less mean diffusion than that of Fig. 3d. This is a consequence of the particles, 100 times greater inertia for the present case shown in Fig. 4d. In general, the $St_\delta = 1$ particles primarily convect downstream while moving away from the wall at their terminal velocity (mostly ignoring the turbulence as they pass).

3.2. Particle concentration distribution

Fig. 5 shows the transverse particle distribution profile for both the constant inertia ($St^+ = 2.7$) study and the constant Froude number ($Fr_\delta = 1$) study at 15 boundary layer thicknesses downstream of injection. In this figure, C represents the concentration of particles in a transverse bin

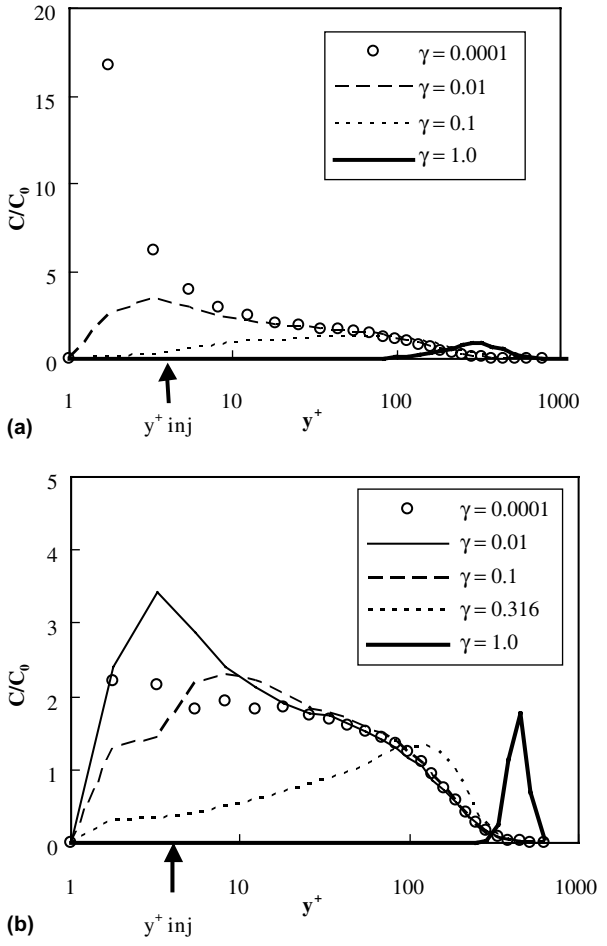

Fig. 5. Normalized concentration profiles at $x^* = 15$ for (a) the constant Stokes number study and (b) the constant Froude number study.

(obtained through net flux statistics) and C_0 is the bulk concentration (equal to the average concentration over all bins containing particles). The y^+ values shown for $\gamma = 10^{-4}$ locate the center of each of the 26 transverse bins, which are used for all cases, and the arrow labeled y^+_{inj} denotes the transverse injection location. Note that the $\gamma = 10^{-3}$ case is omitted in this figure (and others) as it was reasonably represented by the $\gamma = 10^{-4}$ case, i.e. drift parameter effects were found to be generally negligible for $\gamma < 10^{-3}$ (Dorgan and Loth, 2003).

The St^+ for all of the cases shown in Fig. 5a is of order one, implying that they should possess inertial tendencies in the near-wall region (i.e. the particle's response time is too large to allow it to effectively react to the short time-scale turbulent fluctuations in the near-wall fluid). Young and Leeming (1997), as well as Marchioli and Soldati (2002) noted that this condition leads to particles becoming trapped in the near-wall region through the turbophoresis effect. The turbophoresis phenomenon is caused by gradients in the fluid turbulence and acts to carry particles away from the peak turbulence location. As such, particles released at $y^+ = 4$ will be in a region where transverse velocity fluctuations increase away from the wall (Fig. 1c) and will therefore be moved toward the wall if terminal velocity effects are negligible. This "trapping" feature is evident in the distribution profile as a large near-wall peak is seen at $y^+ = 2$ for the smallest γ condition at $x^* = 15$. Additionally, the 10^{-1} case yields a leg that tends to flatten out smoothly in the outer regions of the boundary layer where St_δ is the governing parameter and where the particle should behave as a passive scalar since $St_\delta \ll 1$.

Increasing the drift parameter essentially increases the strength of the terminal velocity (directed away from the wall) and pulls the particles away from the near-wall structures of the turbulence. As such, the effect of turbophoresis (a near-wall, inertial phenomenon) competes with the strength of the terminal velocity in determining the particle cloud's transverse movement. For example, the $\gamma = 10^{-2}$ case has a peak concentration at $y^+ \sim 3$ shifted towards the wall due to turbophoresis. However, as γ increases, the terminal velocity is sufficiently large that many of the particles are pulled to the outer regions of the boundary layer where they are capable of diffusing like fluid tracers since the effective Stokes number, $\langle St_A \rangle$, is of the order St_δ (and not St^+) in this region. The largest γ case ($\gamma = 1$) has the lowest peak concentration and appears to be the most diffused as the width of the distribution profile is considerably larger than that of the other cases. This is most likely due to its immediate withdrawal from the near-wall region and its abrupt exposure to the larger turbulent scales in the outer regions of the boundary layer.

Fig. 5b shows the particle distribution profile for selected cases with $Fr_\delta = 1$ at $x^* = 15$. As the drift parameter (and Stokes number) increase, the particles generally move away from the wall and have smaller peak concentrations (for both streamwise locations). It should be noted that the smallest particles for the constant Fr_δ study ($St_\delta = \gamma = 10^{-4}$) tend to behave as passive tracers (since their St^+ is much less than unity) and simply move with the fluid—this was not the case for the constant Stokes number study results for $\gamma = 10^{-4}$. Examining the results for $\gamma = 10^{-4}$ shown in Fig. 5a ($St^+ = 2.7$) and Fig. 5b ($St^+ = 0.027$), it is seen that the near-wall concentration in the former case is predominately a result of the inertial effect. This qualitatively supports the postulate by Young and Leeming (1997) that turbophoresis is a function of St^+, and not γ for turbulent wall-shear flows.

The larger cases ($\gamma = 10^{-1}$, 0.316, and 1) have a reduced concentration in the near-wall region when compared to the smallest two cases shown in this figure, and is attributed to their relative magnitudes of terminal velocity. The increase in the drift parameter pulls the particles from the

near-wall region and prevents inertial effects such as turbophoresis from pushing them to the wall. The influence of γ on the largest particle condition is very obvious as the distribution profile peaks in the neighborhood of $y^+ = 400$ (approximately 1.5δ) at $x^* = 15$. The sharper peak, as compared to particles of lesser γ, indicates a reduction in diffusion caused by the increase in the crossing trajectory effect. Additionally, this reduced diffusion (as compared to the $\gamma = 1$ case of Fig. 5a) is a

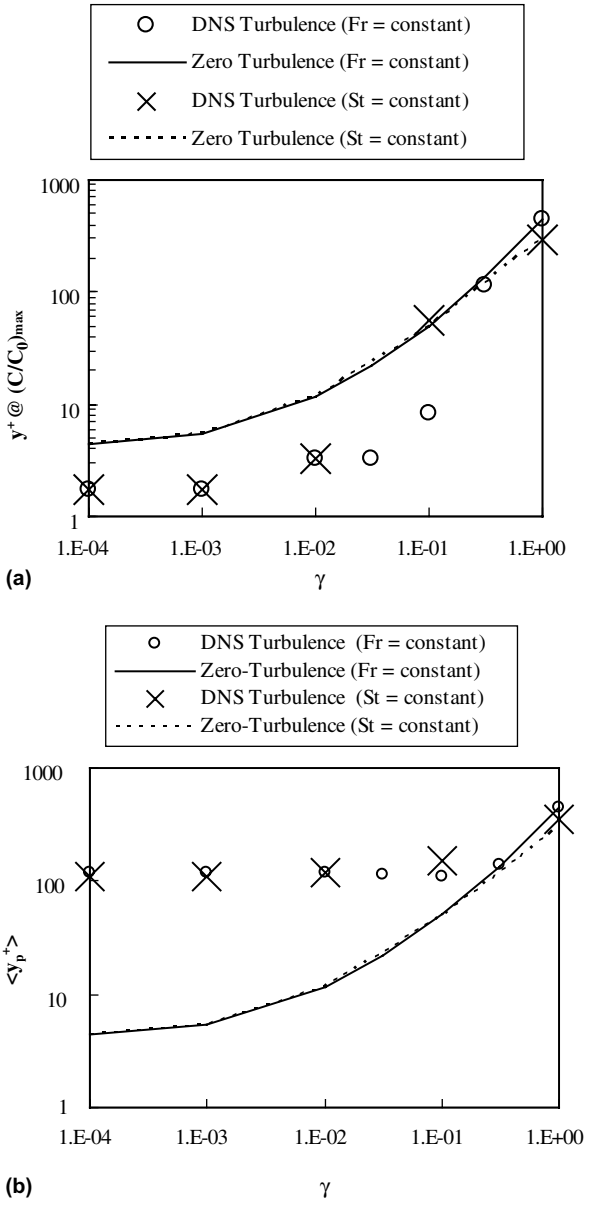

Fig. 6. Location of (a) maximum particle concentration and (b) mean particle trajectory at $x^* = 15$.

result of the high inertia of the particle ($St_\delta = 1$), which causes the initial short-term diffusion rates to be significantly reduced (as noted in Section 1).

Fig. 6a shows the transverse location of the peak concentration at $x^* = 15$ for the entire range of γ for both the constant Stokes number and constant Froude number simulations when subjected to the turbulence field of the DNS solution. Additionally, a "zero-turbulence" curve is given for both cases. This zero-turbulence data was collected by integrating the particle equation of motion using only the mean flow-field of the DNS solution, i.e. using only $[u_{fi}]$ and neglecting the fluctuating $u'_{fi}(t)$. As such, all particles in the zero-turbulence field followed identical trajectories and yielded a Dirac delta function for the concentration profile. In general, the peak concentration locations for the zero-turbulence simulations are primarily a function of the drift parameter, where an increase in terminal velocity leads to an increase in mean transverse path location. Note that after moving 15δ downstream, the particle locations in the zero-turbulence case for $\gamma = 10^{-4}$ are still very near the transverse injection location of $y^+ = 4$, since they move by the influence of $[v_f]$ and V_{term} alone, both of which are quite small for this condition.

Now let us consider the DNS trends where the particle trajectories include the effects of turbulence. In general, the peak location increases with increasing γ (as in the zero-turbulence case). However, the smallest γ values have peak locations very near the wall (e.g. $y^+ = 2$) indicating the influence of the wall boundary condition for the initial concentration evolution (recall Fig. 5). The smallest three γ values (10^{-4}, 10^{-3}, 10^{-2}) for both the constant Froude number ($Fr_\delta = 1$) and constant inertia ($St_\delta = 10^{-2}$) studies have the same peak concentration locations at $x^* = 15$ suggesting that changes in Stokes number at this level are negligible in terms of peak concentration location (though St^+ did have a large effect on peak concentration *magnitude* and overall distribution shape as noted in comparing Fig. 5a and b).

The $\gamma = 10^{-1}$ case shows the largest difference due to Stokes number variation. The smaller Stokes number case ($St^+ = 2.7$) joins the corresponding zero-turbulence curve while the larger Stokes number case ($St^+ = 27$) remains well below its respective zero-turbulence level. This is attributed to a reduction in diffusion caused by the increased inertia of the latter case. As γ is increased to 1.0, the particles are pulled from the near-wall region and the DNS data points coincide with the zero-turbulence curves indicating that the mean particle transverse flux in these cases is dominated by the terminal velocity.

Fig. 6b shows the location of the mean transverse particle trajectory location at $x^* = 15$ for the entire range of γ for both studies. Note that the data shown for the zero-turbulence curves is identical to that presented in Fig. 6a due the absence of turbulent diffusion. Fig. 6b indicates that turbulent diffusion causes the mean particle trajectory to lie on or above that predicted by the zero-turbulence simulation. This is in contrast to the *peak concentration* shown in Fig. 6a, where the DNS data fell on or below that predicted by the zero-turbulence simulation. For a small drift parameter and small Stokes number, the mean transverse location (and thus mean transverse velocity) is approximately constant. This is caused by the diffusion of fluid particles away from the near-wall region and is a byproduct of the injection location, e.g. particles would diffuse equally away from the injection locations if the particles were instead released a distance away from the reflection plane. For large γ values, the terminal velocity begins to dominate the movement away from the wall such that the DNS and zero-turbulence mean trajectories become similar.

3.3. Particle diffusion rates

Fig. 7 shows the spanwise mean-square deviation of the particle's position relative to the injection location. Fig. 7a gives the data for four drift parameters of the constant Stokes number study while Fig. 7b shows the data for five drift parameters of the constant Froude number study. As there is no component of terminal velocity acting in the spanwise direction (i.e. $[z_p - z_0] = 0$) these plots can be directly related to turbulent diffusion. In general, the spanwise diffusion increases with time for Fig. 7a and b. However, in Fig. 7a (constant Stokes number) the diffusion *increased* with γ while in Fig. 7b (constant Froude number) the diffusion *decreased* with increasing γ.

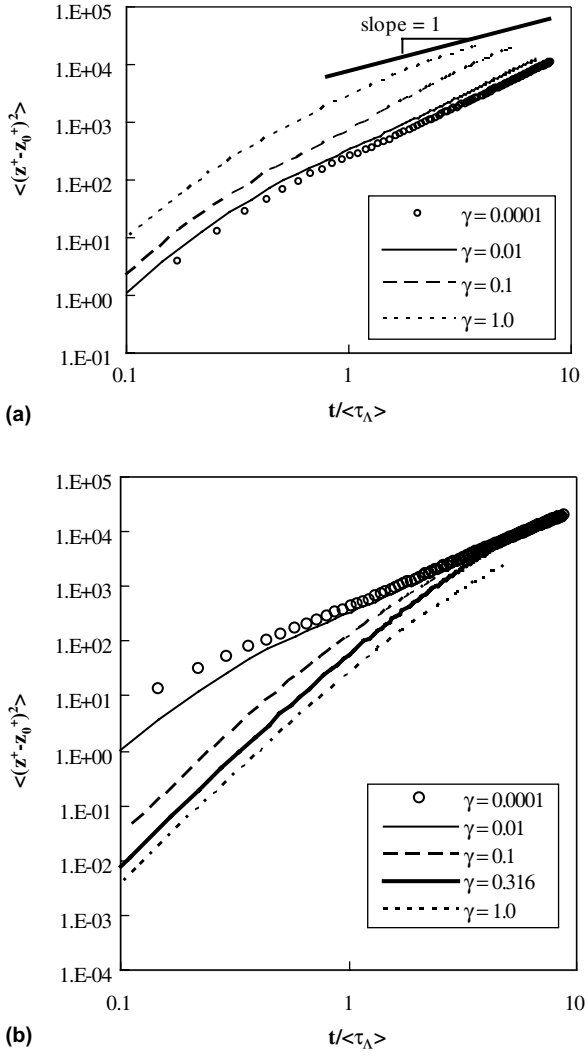

Fig. 7. Spanwise diffusion for (a) constant Stokes number and (b) constant Froude number studies.

To understand this result, it is instructive to first consider the case of $\gamma = 1$ and $St_\delta = 10^{-2}$ of Fig. 7a. Unlike the other γ cases, this particle set will not be significantly affected by near-wall turbophoresis as few particles continue to reside in $y^+ < 70$ (see Fig. 5a). In addition, the particle Stokes number is sufficiently small with respect to the eddies in the outer region that it may be considered to have long-time diffusion as $t/\langle\tau_\Lambda\rangle$ approaches 10. Furthermore, the outer region is approximately homogeneous and isotropic. As such, one should expect the mean-square diffusion to approach a linear variation with time as discussed by Hinze (1959), which is reflected in the Fig. 7a results. As γ is reduced (for $St_\delta = 10^{-2}$, $St^+ = 2.7$) the mean diffusion is reduced since the particles are less likely to reside in the outer region of the boundary layer where τ_Λ is greatest. In addition, the diffusion rate for low γ values tends to be quadratic even at longer times. Thus, the inhomogeneity and anisotropy of the near-wall region significantly modifies the spread rate of the overall particle cloud.

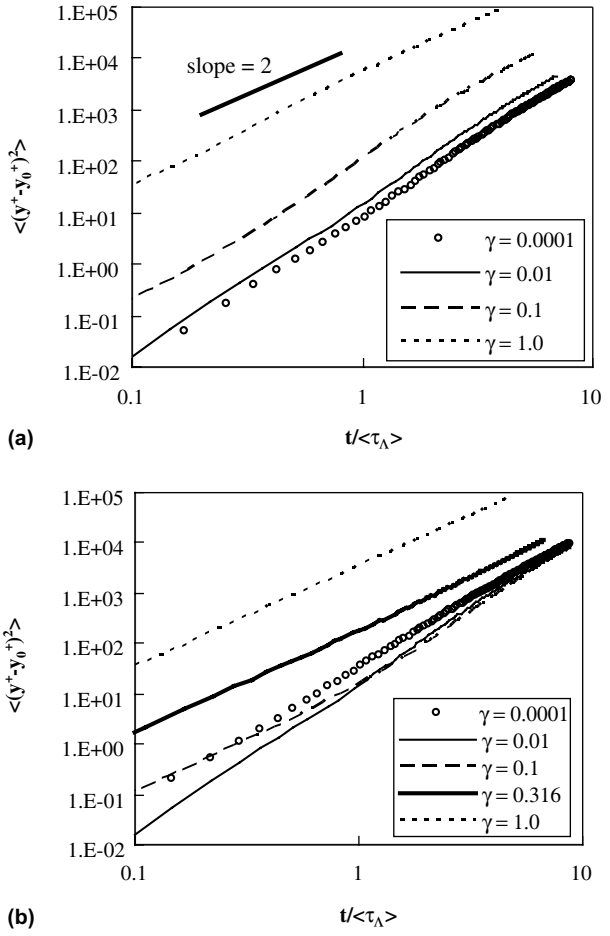

Fig. 8. Transverse mean-square deviation from the injection location for (a) constant Stokes number and (b) constant Froude number studies.

For Fig. 7b, the tracer particles ($\gamma = St_\delta = 10^{-4}$) tend to transition from roughly quadratic diffusion at short-times to nearly linear diffusion at long-times, as expected. However, the increase in γ is associated with an increase in Stokes number. As such, the reduction in the short-time particle diffusion can be expected, owing to the increased inertia and reduced responsiveness of the particles. In fact, the initial diffusion rate for $\gamma = 0.01$ is nearly quartic. This suggests that the crossing trajectories behavior significantly modifies the particle cloud spread rate. For $\gamma = St_\delta = 1$, one can expect that the particle diffusion is generally due to homogeneous, isotropic turbulence once the particles have exited the inner region of the boundary layer, as $t/\langle\tau_\Lambda\rangle$ approaches 10. However, at these times, τ_p is an order of magnitude greater than τ_Λ (see Table 1b) such that one could expect large inertial effects (Hinze, 1959). Thus, short-time diffusion behavior can be expected, consistent with the observed quadratic diffusion rate. Indeed, the mean-square spread tends to obey the classic, short-time quadratic dependence on time as shown in Fig. 7b.

Fig. 8 displays the data from both studies for the transverse mean-square deviation from the injection location for the same cases previously discussed with respect to Fig. 7. In Fig. 8a, little difference is noticed between the 10^{-1} case and the 10^{-2} case. This result is interesting in that it indicates that the slope of mean transverse deviation for all the particles is approximately the same for $\gamma < 10^{-2}$ (and $St_\delta = 10^{-2}$), even though the profiles in the near-wall region showed substantial differences (see Fig. 5a). Thus, examining mean transverse deviation alone obscures the substantial local near-wall turbophoresis effects. Additionally, the largest γ value gives the greatest transverse deviation for the constant Stokes number study and approximately a quadratic slope. This is simply a consequence of the dominance of terminal velocity in carrying particles away from the injection location, i.e. this increase primarily results from $[y_p - y_0] \sim t * V_{term}$.

Fig. 8b gives the transverse mean-square deviation (from the injection location) results for five of the cases considered in the constant Fr_δ study. Interestingly, the $\gamma = 10^{-2}$ and 10^{-1} cases show an overall mean deviation which is somewhat less than the tracer case of $\gamma = 10^{-4}$. This is attributed to the larger particle inertia for these cases and leads to a reduced diffusion rate at short-times. Further increase in γ results in a mean-square value greater than that of the 10^{-1} case simply due to the increased y^+ location caused by terminal velocity (as also noted in Fig. 8a).

3.4. Particle–wall impact velocities

Fig. 9a and b show the horizontal and vertical bounce velocities for both studies normalized by u_τ. These data were collected in a bin stretching from $x^* = 8$ to $x^* = 15$ such that the effect of the initial condition on this statistic will be minimized. In this figure, the absence of a data point implies that no particle in the simulation made contact with the reflection plane imposed at $y^+ = 1$ (e.g. no reflections at either of the $\gamma = 1$ cases). Similar to the results of Uijttewaal and Oliemans (1996), the magnitude of the particle's horizontal and vertical impact velocities were found to generally scale with u_τ. The streamwise and vertical bounce velocities increase with γ up to a value of 10^{-1} which is consistent with the increasing capture distance necessary for wall collision as V_{term} increases (especially at high inertias). Beyond $\gamma = 10^{-1}$ for $Fr_\delta = 1$, Fig. 9 shows that tangential impact velocities increased but vertical impact velocities decreased since these particles cannot respond as quickly to wall trapping velocities (velocities directed towards the wall). Interestingly, the streamwise and transverse bounce velocities are constant and nearly identical in both studies

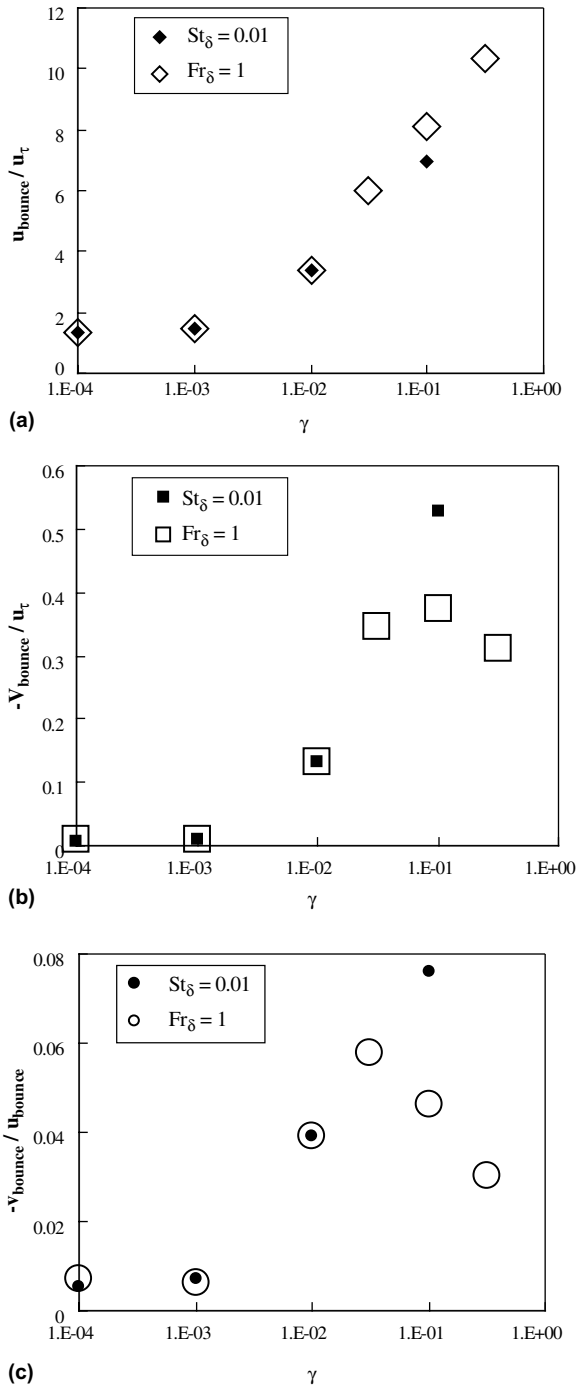

Fig. 9. Bounce velocity statistics: (a) horizontal component, (b) vertical component, and (c) the ratio of components.

for $\gamma \leqslant 10^{-3}$ indicating that the bounce velocities are not dependent on terminal velocity or Stokes number for these conditions. This is consistent with other test conditions (Dorgan, 2003).

Fig. 9c displays the ratio of the bounce velocities and is related to the angle that the particle contacts the reflection plane. For $\gamma \leqslant 0.0316$ the results are virtually identical between the two studies. At $\gamma \leqslant 10^{-3}$, the particles are nearly passive scalars with respect to crossing the $y^+ = 1$ reflection plane and yield small angles due to the low ratio of $v'_{f\,\mathrm{rms}}/u'_{\mathrm{f\,rms}}$ near this plane. At higher γ values, the increased vertical velocity directed toward the wall needed to overcome the higher V_{term} values, caused steeper angles when the particles impact the reflection plane, though the angles remain small (the impact angles range from 0.3° to 4.4°). Once γ and Stokes number are both large ($\langle St_\Lambda \rangle$ greater than unity), there is a reduction in the angle caused by reduced transverse particle velocity fluctuations at high inertias (as previously noted).

3.5. Velocities along the particle trajectory

Fig. 10a shows the vertical particle velocity collected in the DNS flow as well as the vertical particle velocity collected in the zero-turbulence flow, both normalized by V_{term}. These statistics are Lagrangian averages taken over all particle trajectories within the particle tracking domain of Fig. 2, and thus represent the average velocity of the particle cloud as it moves downstream. In considering the zero-turbulence results, it is helpful to recall that these simulations simply involved integrating the particle equation of motion in the mean flow field (neglecting all influence of turbulent fluctuations). As such, in the cases with $\gamma \geqslant 10^{-2}$, $\langle v_{\mathrm{p}} \rangle / V_{\mathrm{term}}$ is approximately equal to one since $V_{\mathrm{term}} \gg [v_{\mathrm{f}}]$. However, for $\gamma = 10^{-3}$, $[v_{\mathrm{f}}]$ at the injection point is approximately $V_{\mathrm{term}}/3$, such that the combination of $[v_{\mathrm{f}}]$ and V_{term} should (and does) result in a particle transverse velocity of approximately 4/3 V_{term}. In the DNS flow (fluid velocity fluctuations present), $\langle v_{\mathrm{p}} \rangle$ is approximately 200 times larger than the terminal velocity for the smallest γ value shown on the plot. This indicates the dominance of turbulent diffusion at moving particles away from the wall when compared to terminal rise velocity effects for $\gamma \ll 1$ (as noted in Fig. 8). As γ increases, the DNS vertical velocities decrease and approach the zero-turbulence curve where the two coincide at the largest γ values, since gravitational effects dominate the mean particle velocity.

Fig. 10b and c show the Lagrangian vertical relative velocity for the constant Stokes number and constant Froude number studies, respectively. If the particles were released in a homogeneous, isotropic turbulent field and no particle reflection condition was imposed at the wall, one would expect the Lagrangian vertical relative velocity to equal the terminal velocity of the particle, i.e. $\langle v_{\mathrm{rel}} \rangle = V_{\mathrm{term}}$, after transients have decayed. Note that a linear drag law and Lagrangian averaging eliminates the bias due to preferential concentration (Wang and Maxey, 1993, Loth, 2000). Notable departures from this behavior are seen in the present study and are found to be related to the transient effects as discussed in the following.

Recall that the particles are injected with the sum of the average Eulerian fluid velocity and the particle's terminal velocity (Section 2.3) and as such, they are not in equilibrium (on average) if there is a mean drift in the transverse fluid velocity observed along the particle path. This phenomenon can be qualitatively demonstrated by constructing an analytical model for particle response to simple sinusoidal fluid velocities. In particular, two sinusoidal fluid velocity profiles 180° out of phase are applied with an initial particle velocity of V_{term} yielding the result (Dorgan, 2003).

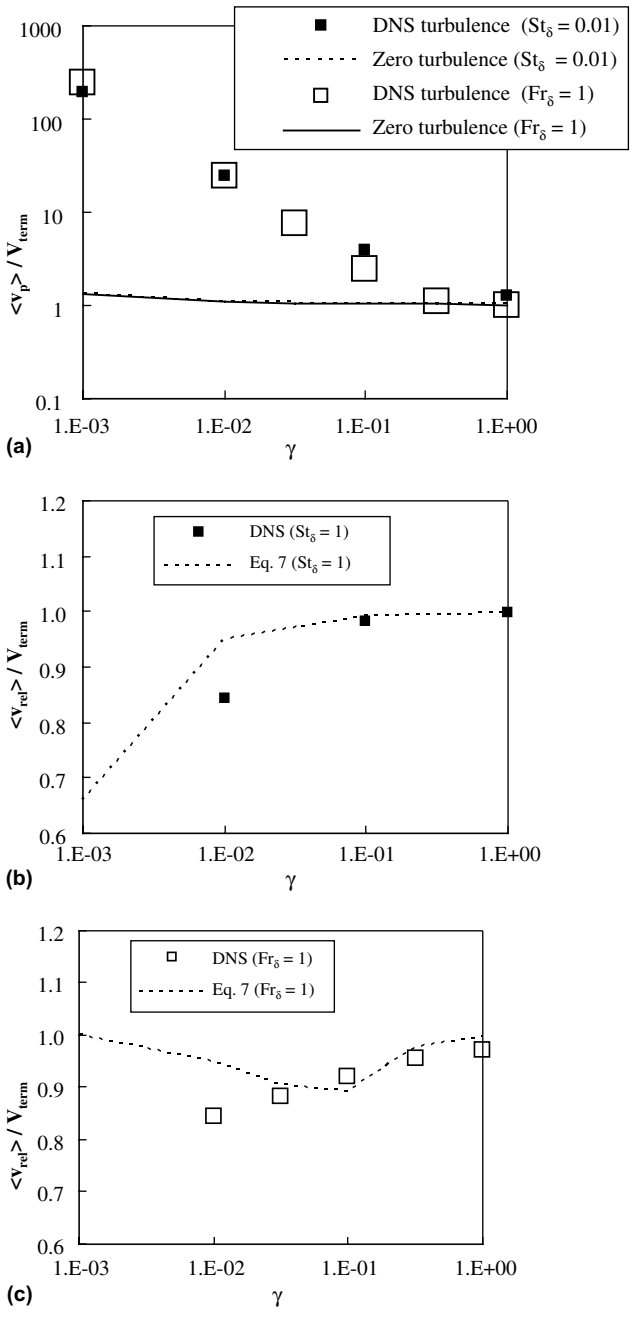

Fig. 10. Lagrangian mean of transverse velocity normalized by the terminal particle velocity: (a) particle velocity, (b) relative velocity for constant Stokes number and (c) relative velocity for constant Froude number.

$$\frac{\langle v_{\mathrm{rel}} \rangle}{V_{\mathrm{term}}} = 1 - \frac{k v'_{\mathrm{f\,rms}}}{b V_{\mathrm{term}}} \int_0^{b\tau_{\mathrm{f}}} \mathrm{e}^{-t/\tau_{\mathrm{p}}}\, \mathrm{d}t \tag{6}$$

In the above expression, "b" is chosen to be an integer and k is a constant used to account for the Lagrangian mean drift in the fluid velocity as seen by the particle. Choosing $b\tau_f$ to be consistent with the integration times given in Table 1 and taking k as the values given by the data of the DNS fluid velocity statistics (Dorgan, 2003) will result in a $\langle v_{rel}\rangle$ less than V_{term}. Note, that if there were no gradient in the Eulerian vertical fluid velocity, we would not expect $\langle v_{rel}\rangle$ to deviate from V_{term}. Application of this model to the constant Stokes number study (where k is approximately constant) predicts that $\langle v_{rel}\rangle/V_{term}$ should approach $-\infty$ as γ becomes much less than one, whereas $\langle v_{rel}\rangle/V_{term}$ should approach unity as γ increases. This is qualitatively consistent with the DNS data (Fig. 10b). For the constant Froude number study, $\langle v_{rel}\rangle/V_{term}$ is approximately predicted as unity for very high γ and very low γ, but a lower $\langle v_{rel}\rangle$ for γ on the order of 10^{-1} due to the combination of transient effects and the mean drift in the Lagrangian fluid velocity.

To complement the mean relative velocity statistics, the fluctuations of the relative velocity were also considered. The root-mean-square (rms) of the relative transverse velocity fluctuations with respect to the Lagrangian mean can be defined as

$$v_{rel,rms} = \left\{ \left\langle (v_{rel} - \langle v_{rel}\rangle)^2 \right\rangle \right\}^{1/2} \tag{7}$$

Fig. 11a shows these fluctuation magnitudes normalized by the Eulerian fluctuation value collected along the particle trajectories ($v'_{f\,rms}$). These results indicate that the fluctuations are approximately constant for the constant Stokes number case but increase for the constant Froude number case. Similar trends were found for the streamwise relative velocity fluctuations, as well as statistics from other DNS cases (Dorgan, 2003 and Dorgan and Loth, 2003). This indicates that the variations are primarily a consequence of changing inertia (St_Λ). For small inertia cases, the relative velocity fluctuations are negligible compared to the turbulence intensity and are of the order of V_{term} (as expected). As the particle inertia becomes large ($St_\Lambda > 1$) the particles tend towards a moving Eulerian trajectory such that fluid turbulent fluctuations will dominate the relative velocity, i.e. $V_{rel,rms} \to V'_{f\,rms}$ for $St_\Lambda \gg 1$. Evidence of this behavior was also given in the channel flow studies of van Haarlem et al. (1998) and Narayanan et al. (2003).

To predict these trends, a simple model was constructed based on the analytical response of the particle's relative velocity subjected to a sinusoidal fluid velocity with zero mean. Dorgan (2003) shows that the relative velocity fluctuations in this case have the following form:

$$\frac{v_{rel,rms}}{v'_{f\,rms}} = \frac{u_{rel,rms}}{u'_{f\,rms}} = \left\{ \left(\frac{\beta St_\Lambda}{1+\beta^2 St_\Lambda^2} \right)^2 + \left(\frac{1}{1+\beta^2 St_\Lambda^2} - 1 \right)^2 \right\}^{1/2} \tag{8}$$

where $\beta = \cos^{-1}(1/e)$. The theoretical predictions are compared with streamwise and transverse velocity results in Fig. 11b indicating reasonable qualitative agreement, despite the inhomogeneous complex nature of the DNS flow.

Finally, the particle Reynolds number is considered as it is of importance when considering the validity of the linear drag-law assumption. As such, Fig. 12 gives the Reynolds number based on both V_{term} and based on the magnitude of the relative velocity averaged along the particle path

$$\langle |Re_p| \rangle = \frac{\langle |\mathbf{V}_{rel}| \rangle d_p}{\nu_f} \tag{9}$$

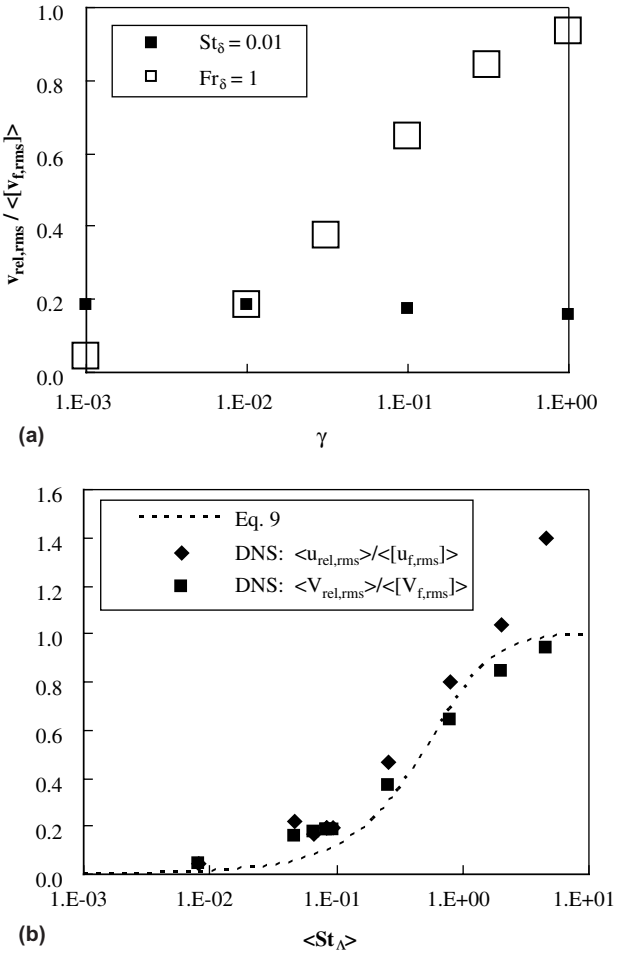

Fig. 11. (a) Relative velocity fluctuation amplitude normalized by the rms of the Eulerian fluctuations along the particle trajectory for the transverse DNS data. (b) A comparison of the DNS data with a theoretical prediction.

where

$$\langle |\mathbf{V}_{\mathrm{rel}}| \rangle = \left\langle \left(u_{\mathrm{rel}}^2 + v_{\mathrm{rel}}^2 + w_{\mathrm{rel}}^2 \right)^{1/2} \right\rangle \tag{10}$$

As a result of its definition, $Re_{\mathrm{p,term}}$ will increase with drift parameter for the present test conditions as demonstrated by the solid lines in Fig. 12. The constant inertia case (Fig. 12a) yields a slope of unity since the fluid viscosity and the particle diameter were held constant while the terminal velocity increases linearly with γ (due to changes in gravity). However, the constant Froude number case has a slope of 1.5 (Fig. 12b) since the particle diameter is also increasing as V_{term} increases.

The results of Fig. 12a indicate that Re_{p} is approximately constant with respect to changes in γ for a given Stokes number (in stark disagreement from the terminal velocity result). This is due to

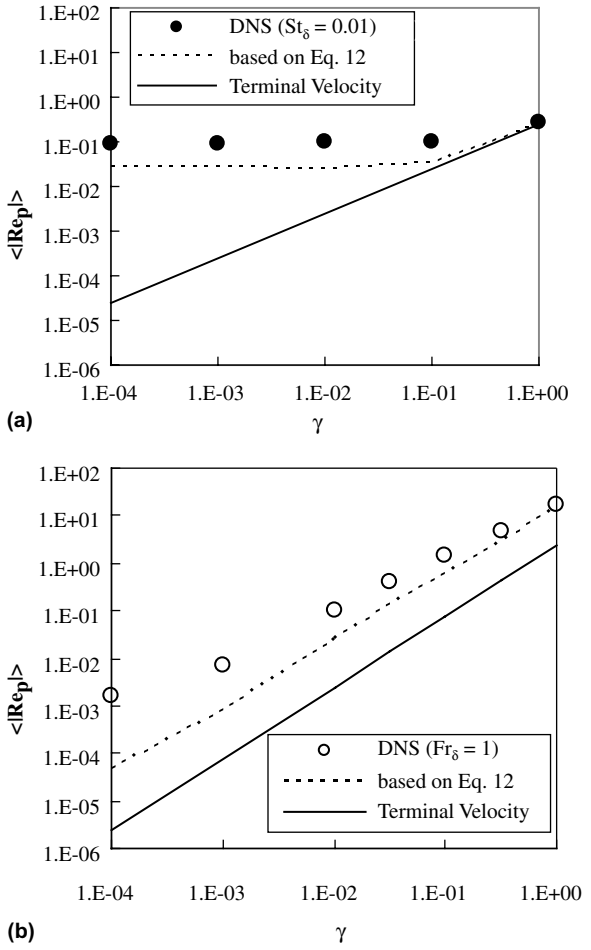

Fig. 12. Particle Reynolds number based on $\langle |V_{rel}| \rangle$ for (a) the constant Stokes number study and (b) the constant Froude number study.

the strong contributions made by the turbulent fluctuations for particle conditions with large ratios of Stokes number to drift parameter (i.e. large Froude numbers). In such cases, the gravitational effects should be expected to be of secondary importance and as such, the Reynolds number based on the terminal velocity is a poor indicator for $\gamma \ll 1$ in these flows. For the constant Froude number results shown in Fig. 12b, it is seen that the DNS particle Reynolds number increases with γ and has approximately the same slope as the $Re_{p,term}$ curve, although it is shifted upwards due to the presence of the finite rms of the relative velocity experienced by the particle in the DNS flow.

To explain these trends, a simple theoretical model was constructed based on results from the zero-turbulence data combined with the Eq. (8) model for the rms velocities, such that

$$|\mathbf{V}_{\mathrm{rel}}|^2 = |\mathbf{V}_{\mathrm{rel,zero\text{-}turbulence}}|^2 + \mathbf{V}^2_{\mathrm{rel,rms}} \tag{11}$$

As shown in Fig. 12, this simple approximation gives a reasonable representation of the results for both the constant Stokes number and constant Froude number simulations, despite inhomogeneous, anisotropic nature of the flow.

4. Conclusions

Simulations have been conducted in a turbulent boundary layer ($Re_\tau = 270$) for a range of particle drift parameters ($10^{-4} \leqslant \gamma \leqslant 10^{0}$) with a fixed inertia (constant Stokes number study, $St_\delta = 10^{-2}$) and then with a variable inertia ($Fr_\delta = 1$). Flow visualization indicated that for nearly fluid tracer conditions (γ and $St^+ \ll 1$), particle ejections from the near-wall region initially correlated strongly with boundary layer ejections of the carrier phase. For higher terminal velocities away from the wall, the correlation was reduced due to the crossing trajectory effect. Additionally, increases in the Stokes number resulted in substantially reduced diffusion and an increase in γ generally results in lower near-wall concentration of particles as the higher terminal velocity tends to remove particles from this region. The concentration profiles near the wall were also affected by changes in the Stokes number since turbophoresis forced particles towards the wall when St^+ was of order unity or greater.

Examination of the spanwise mean statistics showed increased diffusion for increases in γ for constant Stokes number, but decreased diffusion for increasing γ for constant Froude number. These results were attributed to turbophoresis, inertia, and wall interaction effects such that canonical homogeneous, long-time diffusion rates were never fully realized. Similar behavior was noted for the transverse diffusion except that terminal velocity dominated at large γ values.

With respect to particle–wall collisions, the drift parameter was found to be the dominant parameter in determining the impact velocity for $St^+ < 3$ with the present flow conditions where increasing γ yielded increasing velocities. This was attributed the increasing capture distance necessary for collision with the reflection plane even though the terminal velocity was directed away from the wall. However, at larger Stokes numbers, the inertia and injection conditions were found to be influential.

With respect to Lagrangian-averaged velocities, a close coupling was noted between transverse particle velocities and turbulent diffusion for small drift parameters, whereas the terminal velocity dominated the movement as the drift parameter approached unity. In addition, the high inertia particles were seen to experience large relative streamwise velocity fluctuations on the order of the Eulerian fluctuations, whereas the small inertia particles had comparatively lower fluctuations (as the trajectories were more coupled to the fluid unsteadiness). Similarly, particle Reynolds number based on the average of the relative velocity magnitude, $\langle|\mathbf{V}_{\mathrm{rel}}|\rangle$ indicated a transition from being dominated by turbulent diffusion at small drift parameters and small Stokes numbers, to being dominated by the particle's terminal velocity at large drift parameters. The relative velocity fluctuations and the average Reynolds number were reasonably predicted by considering a simple sinusoidal model for the fluctuations in the relative velocity.

Disclaimer

Any opinions, findings, and conclusions or recommendations expressed in this publication are those of the authors and do not necessarily reflect the views of the Defense Advanced Research Projects Agency.

Acknowledgements

This material is based upon work supported by the Defense Advanced Research Projects Agency (DARPA) under grant MDA972-01-C-0042 with Dr. Lisa Porter as Project Manager. Additionally, facilities of the San Diego Supercomputer Center were utilized for the direct numerical simulations. The authors would like to thank Professor P.K. Yeung of the School of Aerospace Engineering at Georgia Tech and Todd L. Bocksell for their valuable comments/input on this publication.

References

Barton, I.E., 1996. Exponential-Lagrangian tracking schemes applied to Stokes law. J. Fluids Eng. 118, 85–89.

Bocksell, T.L., 2003. Numerical simulation of turbulent particle diffusion. Doctoral Dissertation, University of Illinois at Urbana-Champaign.

Brooke, J.W., Kontomaris, K., Hanratty, T.J., McLaughlin, J.B., 1992. Turbulent deposition and trapping of aerosols at a wall. Phys. Fluids A 4, 825–834.

Dorgan, A.J., 2003. Boundary layer dispersion of near-wall injected particles of various inertias. Master of Science Thesis, University of Illinois at Urbana-Champaign.

Dorgan, A.J., Loth, E., 2003. Simluation of particles released near the upper wall in a turbulent boundary layer. Technical Report: AE 03-05, UILU ENG 03-0505.

Hinze, J.O., 1959. Turbulence. McGraw-Hill Book Company.

Kaftori, D., Hetsroni, G., Banerjee, S., 1995. Particle behavior in the turbulent boundary layer. II. Velocity and distribution profiles. Phys. Fluids 7, 1107–1121.

Loth, E., 2000. Numerical approaches to dilute two-phase flow. Prog. Energy Combust. Sci. 26, 161–223.

Marchioli, C., Soldati, A., 2002. Mechanisms for particle transfer and segregation in a turbulent boundary layer. Fluid Mech. 468, 283–315.

Narayanan, C., Lakehal, D., Botto, L., Soldati, A., 2003. Mechanisms of particle deposition in a fully developed turbulent open channel flow. Phys. Fluids 15, 763–775.

Pedinotti, S., Mariotti, G., Banerjee, S., 1992. Direct numerical simulation of particle behavior in the wall region of turbulent flows in horizontal channels. Int. J. Multiphase Flow 18, 927–941.

Spalart, P.R., Watmuff, J.H., 1993. Experimental and numerical study of a turbulent boundary layer with pressure gradients. J. Fluid Mech. 249, 337–371.

Stock, D.E., 1996. Particle dispersion in flowing gases—1994 Freeman scholar lecture. J. Fluids Eng. 118, 4–17.

Uijttewaal, W.S.J., Oliemans, R.V.A., 1996. Particle dispersion and deposition in direct numerical and large eddy simulations of vertical pipe flows. Phys. Fluids 8, 2590–2604.

van Haarlem, B., Boersma, B.J., Nieuwstadt, F.T.M., 1998. Direct numerical simulation of particle deposition onto a free-slip and no-slip surface. Phys. Fluids 10, 2608–2620.

Wang, L-P., Maxey, M.R., 1993. Settling velocity and concentration distribution of heavy particles in homogeneous isotropic turbulence. J. Fluid Mech. 256, 27–68.

Wells, M.R., Stock, D.E., 1983. The effects of crossing trajectories on the dispersion of particles in a turbulent flow. J. Fluid Mech. 136, 31–62.

Young, J., Leeming, A., 1997. A theory of particle deposition in a turbulent pipe flow. J. Fluid Mech. 340, 129–159.